Author's Accepted Manuscript

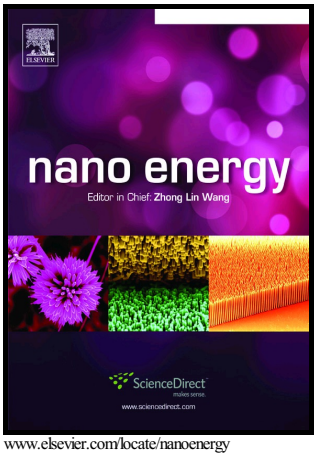

www.elsevier.com/locate/nanoenergy

Effect of Calcination Temperature on the Electrochemical Properties of Nickel-Rich $LiNi_{0.76}Mn_{0.14}Co_{0.10}O_2$ Cathodes for Lithium-Ion Batteries

Jianming Zheng, Pengfei Yan, Luis Estevez, Chongmin Wang, Ji-Guang Zhang

PII: S2211-2855(18)30314-8
DOI: https://doi.org/10.1016/j.nanoen.2018.04.077
Reference: NANOEN2707

To appear in: *Nano Energy*

Received date: 28 February 2018
Revised date: 16 April 2018
Accepted date: 30 April 2018

Cite this article as: Jianming Zheng, Pengfei Yan, Luis Estevez, Chongmin Wang and Ji-Guang Zhang, Effect of Calcination Temperature on the Electrochemical Properties of Nickel-Rich $LiNi_{0.76}Mn_{0.14}Co_{0.10}O_2$ Cathodes for Lithium-Ion Batteries, *Nano Energy,* https://doi.org/10.1016/j.nanoen.2018.04.077

This is a PDF file of an unedited manuscript that has been accepted for publication. As a service to our customers we are providing this early version of the manuscript. The manuscript will undergo copyediting, typesetting, and review of the resulting galley proof before it is published in its final citable form. Please note that during the production process errors may be discovered which could affect the content, and all legal disclaimers that apply to the journal pertain.

ACCEPTED MANUSCRIPT

Effect of Calcination Temperature on the Electrochemical Properties of Nickel-Rich $LiNi_{0.76}Mn_{0.14}Co_{0.10}O_2$ Cathodes for Lithium-Ion Batteries

Jianming Zheng[1*], Pengfei Yan[2], Luis Estevez[1], Chongmin Wang[2], Ji-Guang Zhang[1*]

[1] Energy and Environment Directorate, Pacific Northwest National Laboratory, 902 Battelle Boulevard, Richland, WA 99354, USA

[2] Environmental Molecular Sciences Laboratory, Pacific Northwest National Laboratory, 902 Battelle Boulevard, Richland, WA 99354, USA

*jiguang.zhang@pnnl.gov (J.-G. Zhang)

xmzhjm@126.com (J. M. Zheng)

Accepted manuscript

Abstract

High energy density, nickel (Ni)-rich, layered $LiNi_xMn_yCo_zO_2$ (NMC, $x \geq 0.6$) materials are promising cathodes for lithium-ion batteries. However, several technical challenges, such as fast capacity fading and high voltage instability, hinder their large-scale application. Herein, we identified an optimum calcining temperature range for the Ni-rich cathode $LiNi_{0.76}Mn_{0.14}Co_{0.10}O_2$ (NMC76). NMC76 calcined at 750~775 °C exhibits a high discharge capacity (~215 mAh g^{-1} when charged to 4.5 V) and retains ca. 79% of its initial capacity after 200 cycles. It also exhibits an excellent high-rate capability, delivering a capacity of more than 160 mAh g^{-1} even at a 10C rate. The high performance of NMC76 is directly related to the optimized size of its primary particles (100~300 nm) (which constitute the spherical secondary particles of >10 μm) and cation mixing. Higher calcination temperature (≥800 °C) leads to rapid increase of primary particle size, poor cycling stability, and inferior rate capability of NMC76 due to severe micro-

ACCEPTED MANUSCRIPT

strain and -crack formation upon repeated lithium-ion de/intercalations. Therefore, NMC76 calcined at 750~775 °C is a very good candidate for the next generation of Li ion batteries.

Graphical abstract

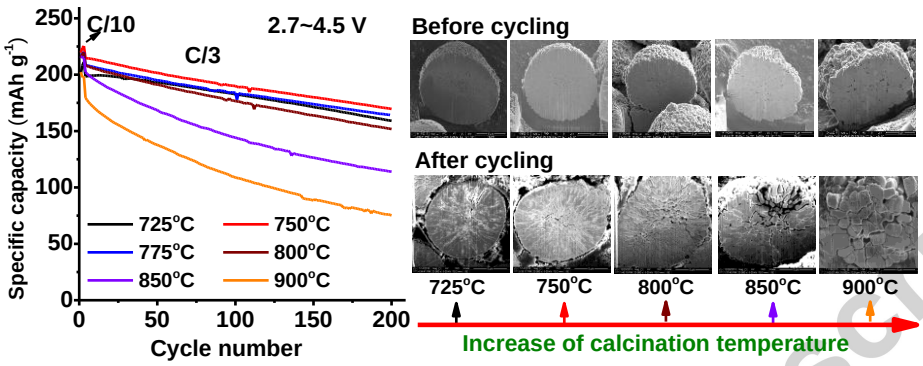

Keywords

nickel-rich cathodes; calcination temperature; cycling stability; micro-strain; crack formation; lithium-ion batteries

1. Introduction

Rechargeable lithium-ion batteries (LIBs) are the dominant power sources for consumer electronics and electric vehicles (EVs) because of their high energy density, light weight, and long cycle life [1-4]. Although significant progress has been made, the driving range of EVs using the state-of-the-art LIBs is still far below those of vehicles using internal combustion engines. The energy density and power capability of LIBs must be improved to increase the driving range and decrease the recharging time. To meet these requirements, significant effort

Accepted manuscript

ACCEPTED MANUSCRIPT

has been made in the search of cathode materials with high discharge capacity and high operating voltage [5-8].

Recently, the Ni-rich, layered-structure cathode material $LiNi_xMn_yCo_zO_2$ (NMC, $x \geq 0.6$) has received much attention due to its high discharge capacity (200~220 mAh g^{-1}) [7-10] and its high energy density (>800 Wh kg^{-1}) compared to traditional $LiCoO_2$ (~570 Wh kg^{-1}) and spinel $LiMn_2O_4$ (~440 Wh kg^{-1}). Ni-rich cathode material also has much higher lithium-ion diffusion coefficients, indicating better power capability than other NMC cathodes with lower Ni content [11]. Another advantage of Ni-rich cathode materials is that their lower Co content reduces production cost. Technical challenges that hinder large-scale application of Ni-rich NMC cathode materials [9,10] include (i) Li/Ni cation mixing due to the difficulty of maintaining all the Ni in the 3+ valence state, (ii) micro-strain and -crack formation caused by significant volume variation during lithium-ion de/intercalation processes, and (iii) safety concern regarding aggressive thermal reactions between the delithiated Ni-rich NMC electrode and the organic carbonate electrolyte.

Significant effort has been dedicated to improving the electrochemical performance and thermal stability of the Ni-rich NMC cathode materials [9]. Representative approaches include lattice doping [12,13], surface treatment/modification [14-17], tuning the material compositions [18], a "smart" design of core-shell or concentration gradient structures [7,8,19], and structural stabilization with low Li_2MnO_3 content [20-22]. Synthetic conditions, such as co-precipitation pH value [23], particle size [23], lithium content [24,25], calcination temperature [26,27], calcination atmosphere (O_2, air, etc.) [28-30], and heating/cooling rates also are important in determining the material's structural properties and thus influencing the electrochemical performance of as-prepared Ni-rich NMC cathode materials. Although the effect of calcination

Accepted manuscript

ACCEPTED MANUSCRIPT

temperature has been reported, most previous study was performed with a low charge cutoff voltage of 4.3 V, which could not fully exploit the advantages of Ni-rich NMC cathodes.

We systematically investigated the effect of calcination temperature on the primary particle size, cation mixing, and electrochemical performance of a Ni-rich cathode material, $LiNi_{0.76}Mn_{0.14}Co_{0.10}O_2$, with a large secondary particle size (>10 μm), which is required to reach a high volumetric density. To obtain high energy density, the $LiNi_{0.76}Mn_{0.14}Co_{0.10}O_2$ materials, calcined at temperatures ranging from 725 to 900 °C, were cycled with a high charge cutoff voltage of 4.5 V. Observations of the structural and interfacial changes in these materials provided insight into the capacity fading mechanism and the relationship between primary particle size and micro-strain generation inside secondary particles of Ni-rich cathode materials.

Accepted manuscript

2. Experimental

2.1. Material preparation and characterization

Spherical, Ni-rich $Ni_{0.76}Mn_{0.14}Co_{0.10}(OH)_2$ precursor was prepared by a mixed hydroxide co-precipitation method, using a continuously stirred tank reactor (CSTR) under N_2 atmosphere. Initially, the CSTR of 5 L capacity was filled with 1.5 L distilled water. Then, an aqueous solution composed of $NiSO_4$, $MnSO_4$, and $CoSO_4$ with a total concentration of 2.0 mol L^{-1} was continuously pumped into the CSTR. At the same time, NaOH solution (8.0 mol L^{-1}) (as the precipitation reagent) and NH_4OH solution (10 mol L^{-1}) (as chelating agent) were also fed into the CSTR separately. The pH value (pH = 11.5), stirring speed (1000 rpm), and temperature (50 °C) were carefully controlled during the precipitation reaction. The precursor was filtered, thoroughly washed with distilled water, and dried overnight at 110 °C. $LiNi_{0.76}Mn_{0.14}Co_{0.10}O_2$ cathode materials were prepared by mixing the $Ni_{0.76}Mn_{0.14}Co_{0.10}(OH)_2$ precursor with LiOH,

ACCEPTED MANUSCRIPT

followed by precalcining at 500 ^{o}C for 10 h and then calcining at temperatures ranging from 725 to 900 ^{o}C for 20 h in ambient air atmosphere. 3 mol% excess Li was used to compensate the loss of Li during calcination at high temperatures. The ramping rates were 3 ^{o}C for heating and 2 ^{o}C for cooling. Calcination is performed in ambient air atmosphere and 5 g of sample material was prepared for each calcination temperature.

Powder X-ray diffraction (XRD) was performed on a Rikagu MiniFlex II apparatus with Cu Kα radiation operated at 30 kV and 15 mA. Data were collected in the 2θ range of 10–90° at 0.1 ° per min. Lattice parameter were refined by the Rietveld method with the General Structure Analysis System (GSAS program, Los Alamos National Laboratory, USA). The refinement was performed on the basis of the α-$NaFeO_2$-type hexagonal structure (R-3m) where the Li ions occupy the 3a (0, 0, 0.5) sites; Ni, Mn, and Co occupy the 3b (0, 0, 0) sites; and O is at the 6c (0, 0, z_{oxy}) sites ($z_{oxy} \approx 0.25$). The morphology of the prepared materials was characterized using a dual focused ion beam (FIB) scanning electron microscope (SEM) (FEI Quanta environmental). Part of the particle was removed by FIB to observe the cross-sectional morphology of Ni-rich NMC materials before and after cycling. Surface areas of the samples were determined with the Brunauer, Emmett, and Teller (BET) method using N_2 adsorption/desorption data collected with a Quantachrome Autosorb 6-B gas sorption system. Scanning transmission electron microscope (STEM) observations were implemented on a probe-aberration-corrected FEI Titan STEM and image-corrected FEI environmental transmission electron microscope (ETEM) at 300 kV. The image intensity of each atomic column reflects the related average atomic number ($\sim Z^{1.5}$ to $Z^{1.8}$) [31], enabling us to visually observe the atomic level structural characteristics.

2.2. Electrochemical measurements

Accepted manuscript

ACCEPTED MANUSCRIPT

Electrochemical performance measurements were conducted using R2032 coin-type cells. The electrodes were prepared by casting a slurry containing 80% active material, 10% polyvinylidene fluoride binder (PVDF, Kureha L#1120), and 10% Super P onto an Al current collector foil. A typical loading of the electrodes was about 4–5 mg cm^{-2}. Thick electrodes with high areal capacity of 2.5 mAh cm^{-2} (~12 mg cm^{-2}) were also prepared, by coating a slurry mixture containing 92% active material, 4% PVDF, and 4% Super P binder onto Al foil. After drying, the electrodes were punched into disks with area of 1.27 cm^2. Electrochemical cells were assembled with the cathodes as prepared, metallic lithium foil as anode, Celgard 2500 (polypropylene) as separator, and 1 M $LiPF_6$ dissolved in ethyl carbonate and dimethyl carbonate (1:2 in volume) as electrolyte. The samples were prepared in an argon-filled glove box (Mbraun, Germany) where both oxygen and moisture content were controlled below 1 ppm. Charge-discharge experiments were performed galvanostatically between 2.7 and 4.5 V on an Arbin BT-2000 battery tester at 30 °C and 60 °C. The rate capability was evaluated using the same charge rate of C/5 and a gradual increase in the discharge C rate after the initial five charge/discharge cycles at C/10 rate. A 1C rate corresponds to a current density of 200 mA g^{-1} in this work. Electrochemical impedance spectra (EIS) measurements were performed using a Solartron 1255B frequency analyzer and 1287 electrochemical workstation in a frequency range from 100 kHz to 1 mHz with a perturbation amplitude of ±10 mV.

Accepted manuscript

3. Results and Discussion

Fig. 1 shows the XRD patterns and the refinement results of the $LiNi_{0.76}Mn_{0.14}Co_{0.10}O_2$ cathodes calcined at different temperatures ranging from 725 to 900 °C. The synthesized samples are all phase-pure without any impurity detected (Fig. 1a). All the diffraction peaks of the XRD

ACCEPTED MANUSCRIPT

pattern could be indexed to the layered hexagonal structure of α-$NaFeO_2$ with space group R-3m. The clear splitting of the (006) and (012) peaks and of the (018) and (110) peaks indicates a well-ordered, layered structure. The full width at half maximum (FWHM) of (003) XRD peaks decreases with increase of calcination temperature (Fig. 1b), revealing a growth of crystallite size in the synthesized materials. The crystallite size is estimated based on the Scherrer equation, $L = k\lambda/(\beta\cos\theta)$, according to the FWHM of (003) diffraction peaks [32], where k is a constant related to crystallite shape and normally taken as 0.89, λ is 0.15406 nm, and β is FWHM of the diffraction peak in a 2θ scale. The results show that the crystallite size increases from 27.5 nm for material prepared at 725 °C to 46.8 nm for material prepared at 900 °C, as shown in Table 1. Rietveld refinement of the XRD data was done to obtain the lattice parameters and the Li/Ni cation disorder. The results are summarized in Table 1, and the representative refinement patterns of materials prepared at 750 °C and 775 °C are presented in Fig. 1c, d, while those of the materials prepared at other temperatures are shown in Fig. S1. All the refinements show good fit between the observed and calculated patterns. The calculated ***a*** and ***c*** lattice parameters slightly increase for materials calcined at higher temperatures during preparation, which could be ascribed to the enhanced crystallinity of the prepared materials.

Accepted manuscript

ACCEPTED MANUSCRIPT

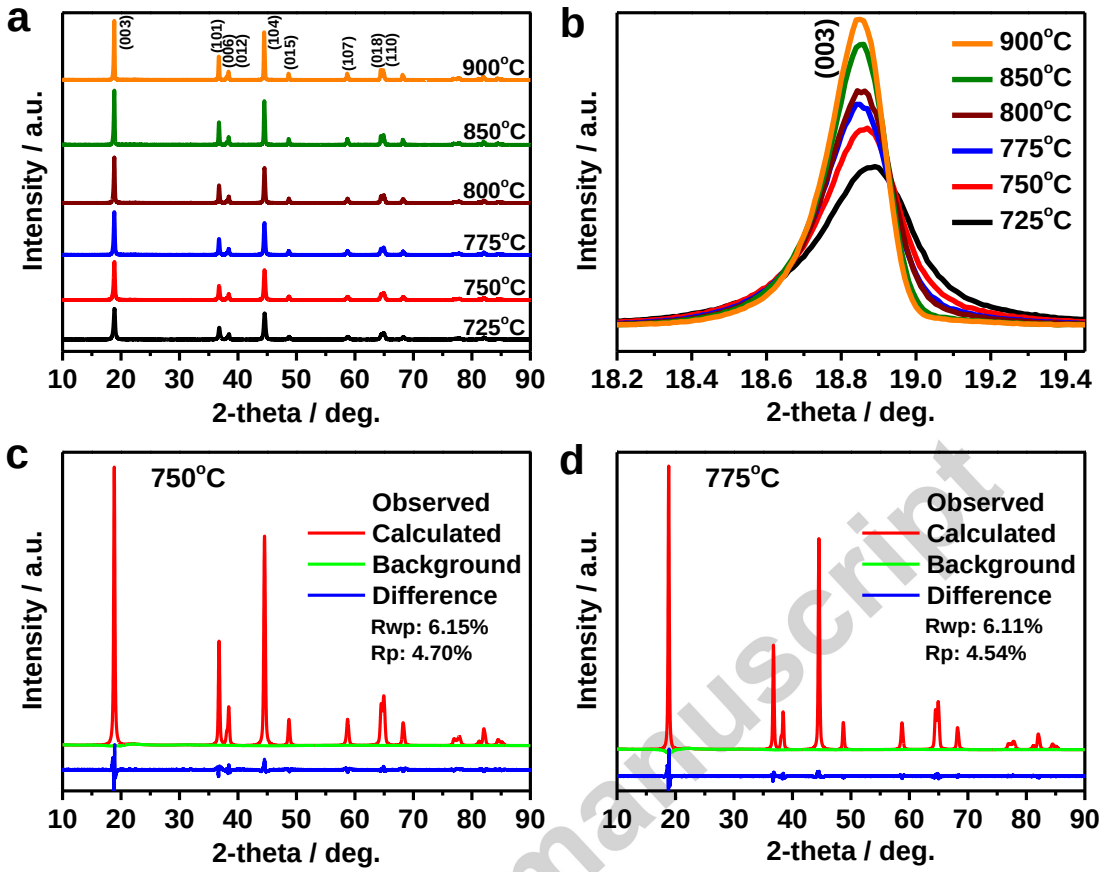

Fig. 1. (a) XRD patterns and (b) (003) diffraction peaks of the $LiNi_{0.76}Mn_{0.14}Co_{0.10}O_2$ cathodes calcined at different temperatures. (c, d) Rietveld refinement results of $LiNi_{0.76}Mn_{0.14}Co_{0.10}O_2$ cathodes prepared at (c) 750 °C and (d) 775 °C.

The degree of Li/Ni cation mixing was calculated assuming that some Ni ions may occupy Li sites because the ionic radius of Ni^{2+} (0.69 Å) is similar to that of Li^{+} (0.76 Å). Overall, the Li/Ni cation mixing in $LiNi_{0.76}Mn_{0.14}Co_{0.10}O_2$ cathodes calcined at different temperatures is in the range of 3~5%. Li/Ni cation mixing decreases with increase of calcination temperature, and reaches a minimum value at 775 °C (3.65%), which could be due to the improvement in crystallinity at 775 °C, as shown in Fig. 1b. The highest intensity ratio ($I_{(003)}/I_{(104)}$) between the (003) and (104) diffraction peaks of the material prepared at 775 °C (1.33, Table 1) further confirms the superior layered-structure properties of the material [23,33].

Accepted manuscript

ACCEPTED MANUSCRIPT

However, further increase of calcination temperature to 900 °C creates more Li/Ni cation mixing despite the enhanced crystallinity. This could be attributed to an increase of oxygen vacancies at high calcination temperature, which induces formation with a slightly higher content of Ni^{2+}, and thus results in more Li/Ni cation mixing. Therefore, a compromise between structural crystallinity and cation disorder will be needed when optimizing the calcination temperature for Ni-rich cathode materials.

Table 1. Crystallographic data derived from Rietveld refinements, and BET surface area of the $LiNi_{0.76}Mn_{0.14}Co_{0.10}O_2$ cathodes calcined at different temperatures.

Temperature	**725 °C**	**750 °C**	**775 °C**	**800 °C**	**850 °C**	**900 °C**
a-axis (Å)	2.877(0)	2.877(1)	2.877(2)	2.878(1)	2.878(6)	2.880(3)
c-axis (Å)	14.228(0)	14.228(8)	14.230(4)	14.233(3)	14.235(4)	14.239(1)
Grain size (nm)	27.5	31.8	34.6	37.9	41.9	46.8
Ni in Li sites (%)	4.94	4.79	3.65	4.06	4.48	5.16
$I_{(003)}/I_{(104)}$	1.17	1.26	1.33	1.28	1.23	1.23
BET surface area ($m^2\ g^{-1}$)	0.225	0.358	0.319	0.334	0.249	0.518

Accepted manuscript

SEM images of the $LiNi_{0.76}Mn_{0.14}Co_{0.10}O_2$ cathodes calcined at different temperatures are shown in Fig. 2. To assure a reliable evaluation of the effect of calcination temperature on the properties of Ni-rich $LiNi_{0.76}Mn_{0.14}Co_{0.10}O_2$ cathodes, the same batch of spherical NMC hydroxide precursor was used for the material preparation. The synthesized materials retain well the spherical morphology of the precursor (Fig. 2a1, b1…f1), even though particle shape deformation and shrinkage are observed for samples prepared at calcination temperatures above

ACCEPTED MANUSCRIPT

850 °C (Fig. 2e1, f1). When the materials are prepared at 725~775 °C, there is no clear difference in the size of primary particles, which is about 100~300 nm. However, further increase of the calcination temperature to ≥800 °C gives rise to a significant growth of primary particles, increasing from ca. 500 nm for 800 °C to ca. 1 μm and ca. 2 μm for materials prepared at 850 °C and 900 °C, respectively. Large primary particle size will extend the length of lithium-ion diffusion pathways and result in inferior rate performance. We also used a FIB to section the particle material for cross-sectional SEM observation. The SEM images in Fig. 2a3, b3…e3 and Fig. S2 demonstrate that the secondary particles of the materials are densely compacted with few voids inside the particles. When prepared at higher calcination temperature, i.e., 900 °C, the material shows explicit grain boundaries between large primary particles, along with enlarged void space inside the secondary particles (Fig. f3).

Accepted manuscript

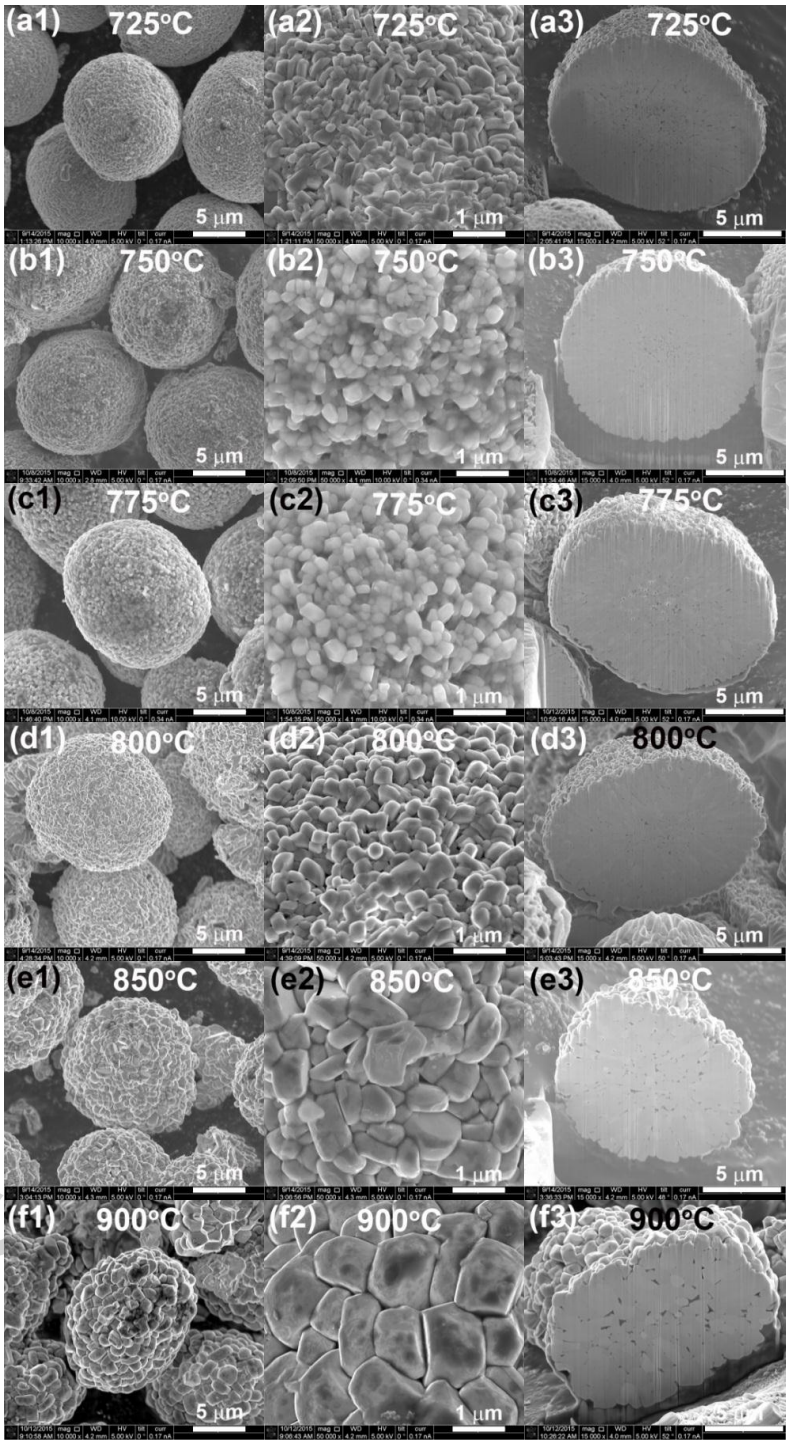

Fig. 2. Surface and cross-sectional SEM images of $LiNi_{0.76}Mn_{0.14}Co_{0.10}O_2$ cathodes prepared at different calcination temperatures: (a1–a3) 725 °C, (b1–b3) 750 °C, (c1–c3) 775 °C, (d1–d3) 800 °C, (e1–e3) 850 °C, and (f1–f3) 900 °C.

ACCEPTED MANUSCRIPT

To evaluate the effect of calcination temperature on the electrochemical performance of Ni-rich $LiNi_{0.76}Mn_{0.14}Co_{0.10}O_2$ cathodes, the electrodes were cycled with a charge cutoff voltage of 4.5 V, and the results are shown in Fig. 3. As presented in Fig. 3a, b, the material prepared at a relatively low temperature of 725 °C shows the lowest charge/discharge capacity and a slightly lower discharge voltage profile, which is consistent with its relatively poor crystallinity. On the other hand, the material prepared at a relatively high temperature of 900 °C shows similar charge capacity to the other materials but lower discharge capacity of 202 mAh g^{-1}, indicating a relatively poor coulombic efficiency (83.8%), which could be due to the greatly increased lithium-ion diffusion distance in the large primary particles (ca. 2 μm). The other materials, prepared at temperatures between 750~850 °C, show almost overlapping charge/discharge voltage profiles and deliver similar discharge capacities of about 215 mAh g^{-1} with initial coulombic efficiency of ca. 88%. The energy density of the $LiNi_{0.76}Mn_{0.14}Co_{0.10}O_2$ cathode is estimated to be as high as 849 Wh kg^{-1} based on the discharge voltage profile in lithium half-cells (see Fig. 3b), which is comparable to the best value reported for layered oxide cathode materials [30].

During cycling at C/3 rate, the materials show obvious differences in terms of discharge capacity as a function of cycle number, as shown in Fig. 3a. It is interesting that the capacity retention (after 200 cycles) of the materials decreases continuously with increasing calcination temperature, being 80.1%, 79.0%, 78.7%, 72.9%, 56.4%, and 41.9% for materials prepared at 725, 750, 775, 800, 850, and 900 °C, respectively. Even though the material prepared at 725 °C shows the best capacity retention, its low reversible capacity makes it less attractive for practical applications. For conventional NMC cathode materials, i.e., $LiNi_{1/3}Mn_{1/3}Co_{1/3}O_2$ and $LiNi_{0.4}Mn_{0.4}Co_{0.2}O_2$, calcination temperature ≥900 °C is usually used to obtain final materials

Accepted manuscript

ACCEPTED MANUSCRIPT

with improved crystallinity and good performance [34,35]. However, Ni-rich cathode materials are quite sensitive to the calcination temperature used in material preparation. A calcination temperature above 800 °C is often detrimental to the electrochemical performance despite the good crystallinity it produces. In comparison, the materials prepared at 750 and 775 °C exhibit superior reversible capacity during cycling, and are still capable of delivering high discharge capacities of 170 and 164 mAh g^{-1} after 200 cycles. Based on the discharge capacity and long-term cycle life, the optimal calcination temperature for the synthesis of Ni-rich cathode material $LiNi_{0.76}Mn_{0.14}Co_{0.10}O_2$ is 750~775 °C.

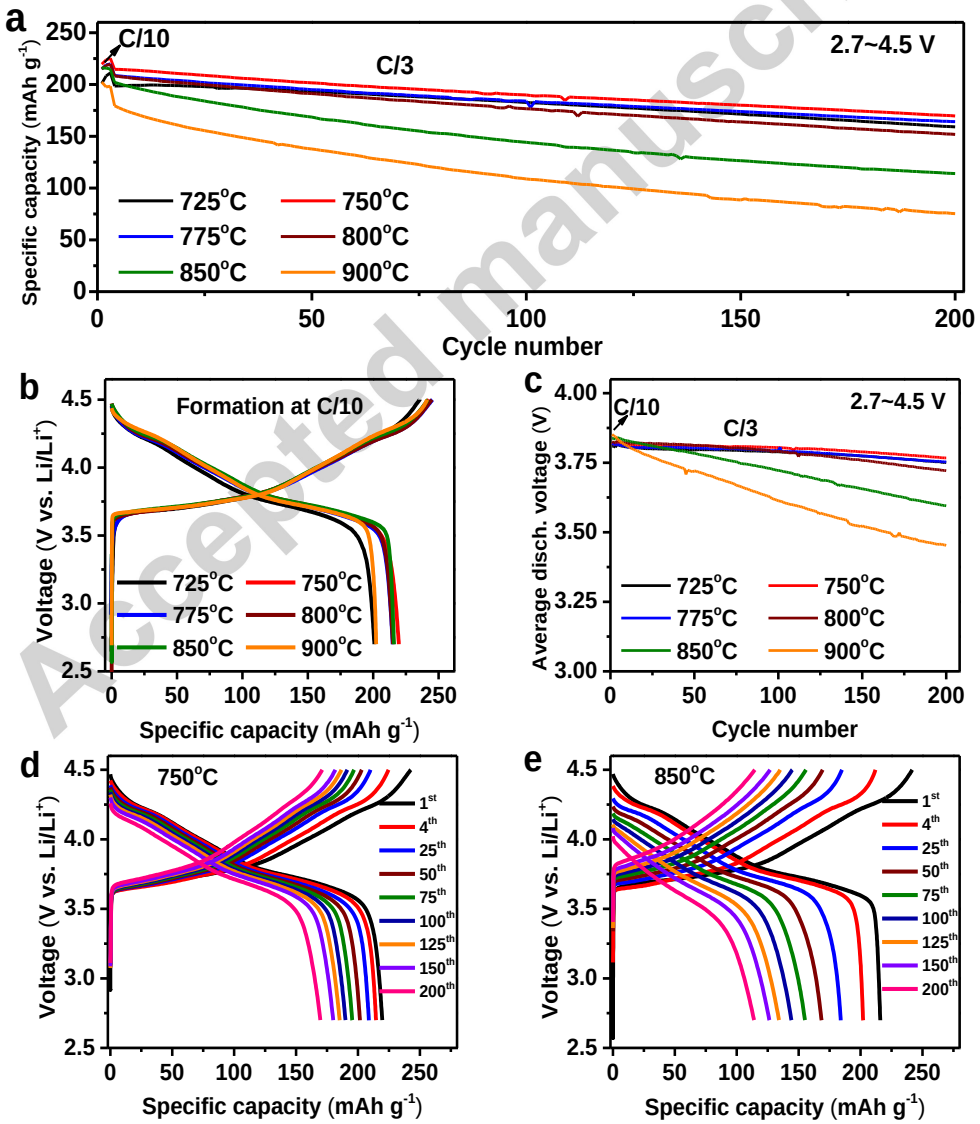

Accepted manuscript

ACCEPTED MANUSCRIPT

Fig. 3. (a) Cycling performance, (b) initial charge/discharge profiles (at C/10), and (c) average discharge voltages of the $LiNi_{0.76}Mn_{0.14}Co_{0.10}O_2$ cathodes calcined at different temperatures and cycled at C/3 after 3 formation cycles at C/10 between 2.7~4.5 V at 30 °C. Charge/discharge voltage profile evolutions of $LiNi_{0.76}Mn_{0.14}Co_{0.10}O_2$ calcined at (d) 750 °C, and (e) 850 °C.

Because of the structural and interfacial instability of Ni-rich materials, all of these materials show continuous voltage decay during cycling. The evolution of average discharge voltages of $LiNi_{0.76}Mn_{0.14}Co_{0.10}O_2$ cathodes calcined at different temperatures is summarized in Fig. 3c, while the charge/discharge voltage profile evolutions are compared in Fig. 3d, e, and Fig. S3. The data demonstrate that the $LiNi_{0.76}Mn_{0.14}Co_{0.10}O_2$ calcined at 750 °C (Fig. 3c, d) exhibits only 0.055 V decay in average discharge voltage after 200 cycles. This voltage decay is much less than 0.105, 0.242, and 0.399 V, respectively, for materials calcined at temperatures of 800, 850, and 900 °C (Fig. 3c, e). The voltage decay profile of Ni-rich cathode materials is slightly different from those observed for Li-rich, Mn-rich cathode materials, which show voltage decay mainly during the latter part of discharge due to the phase transformation from layered to spinel-like/rock-salt phase [36,37]. The apparent absence of voltage plateaus at around 3 V in the charge/discharge voltage profiles rules out the formation of a Mn-enriched spinel-type phase after cycling. In this regard, although there would still be phase transformation occurring at the particle surface, the overall voltage profile decay observed in Ni-rich cathodes (e.g., 900 °C sample) would be mainly ascribed to the increase of interfacial resistance caused by parasitic side reactions as well as the loss of particle/particle contact because of crack formation [14].

The fundamental mechanism underlying the capacity fading and voltage profile decay was further investigated. To understand the electrochemical performance difference of the

Accepted manuscript

materials calcined at different temperatures, the cells were disassembled after 200 cycles and the cathodes were retrieved for further characterization. Here, we focused on examining the micro-strain and micro-crack formation in the cycled particles. Cross-sectional SEM images of the cycled particles shown in Fig. 4 reveal the formation of micro-cracks and void space inside the cycled particles. Micro-strain and micro-cracks induced by electrochemical cycling have been reported for other Ni-rich cathode materials, such as $LiNi_{0.8}Co_{0.15}Al_{0.05}O_2$ [38,39], $LiNi_{0.6}Mn_{0.2}Co_{0.2}O_2$ [14], and full-concentration-gradient Ni-rich cathode [40]. The crack formation is ascribed to the stress arising from the anisotropic lattice expansion and contraction of different grains inside a secondary particle upon Li^+ ion extraction/insertion, which causes significant micro-strain at the grain boundaries [39,41].

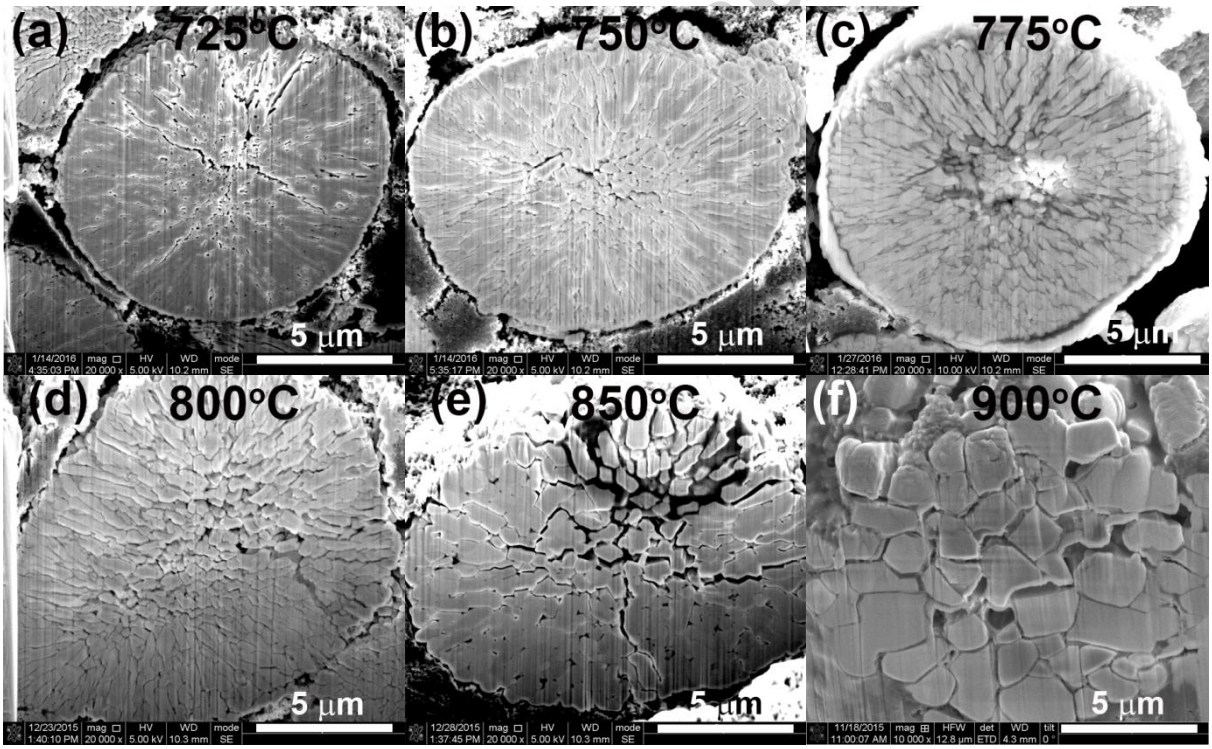

Fig. 4. SEM images of the $LiNi_{0.76}Mn_{0.14}Co_{0.10}O_2$ cathodes prepared at different calcination temperatures after 200 cycles at C/3 in the voltage range of 2.7~4.5 V. (a) 725 °C, (b) 750 °C, (c) 775 °C, (d) 800 °C, (e) 850 °C, and (f) 900 °C.

ACCEPTED MANUSCRIPT

The materials calcined at different temperatures show different degrees of crack formation, which becomes more substantial and serious with increase of calcination temperature. This phenomenon is believed to be closely related to the size of the primary particles constituting the secondary particles of each material, which is a critical factor affecting the crack formation [42]. The materials calcined at relatively low temperatures, i.e., 725~775 °C, are composed of well-aligned nanoplate particles, which generate less micro-strain during each Li^+ ion extraction/insertion process. Therefore, few cracks and voids are observed in these materials (Fig. 4a-c), which correlates well with their superior long-term cycle life, as shown in Fig. 3. In contrast, the materials prepared at higher temperatures, i.e., 800~900 °C, exhibit serious cracks and voids inside the particles because of the substantial micro-strain caused by anisotropic volume variation (Fig. 4d-f). This phenomenon is also in good agreement with those observed by Sun et al. [40] and further supported by our capacity fading mechanism study of $LiNi_{0.76}Mn_{0.14}Co_{0.10}O_2$ prepared at 750 ^oC. As shown in Fig. 5, the pristine material (prepared at 750 ^oC) is composed of densely compacted primary particles which show well defined R-3m layered structures (Fig. 5a-c). Although the materials prepared at lower temperature (e.g. 750 ^oC) exhibit much smaller micro-strain during cycling than those prepared at higher temperatures (e.g. 900 ^oC), after cycling, the primary particles still lose contact with each other due to the anisotropic volume variation at deep lithium extraction and insertion (Fig. 5d). As the cracks form, the electrolyte penetrates into the interiors of secondary particles along the crack network, leading to the formation of a resistive solid electrolyte interphase (SEI) layer at the grain boundaries (Fig. 5e). Moreover, a small portion of the original layered structures at the outer surface of material particle transforms to Ni-O type rock salt phase, leading to the blockage of fast lithium ion transportation pathways. Crack formation and the degradation of particle

Accepted manuscript

ACCEPTED MANUSCRIPT

interfacial stability result in loss of electrical contact between the primary particles, leading to quick buildup of electrode resistance and fast capacity fading. Based on the microscopy observation and electrochemical performances, the optimized primary particle size of Ni-rich NMC is determined to be 100~300 nm, in order to achieve the superior electrochemical performances. If the primary particle size exceeds the critical value [43], in present case ~1 μm, much higher internal strain would be generated and serious particle cracking will occur during cycling. This is considered the primary reason for the poor cycling stability of the Ni-rich materials calcined at temperatures above 800 °C due to their large primary particles. Therefore, mitigation of the micro-strain and -crack formation in the secondary particles by tuning the primary particle size is critically important for achieving improved long-term cycling stability of these cathode particles.

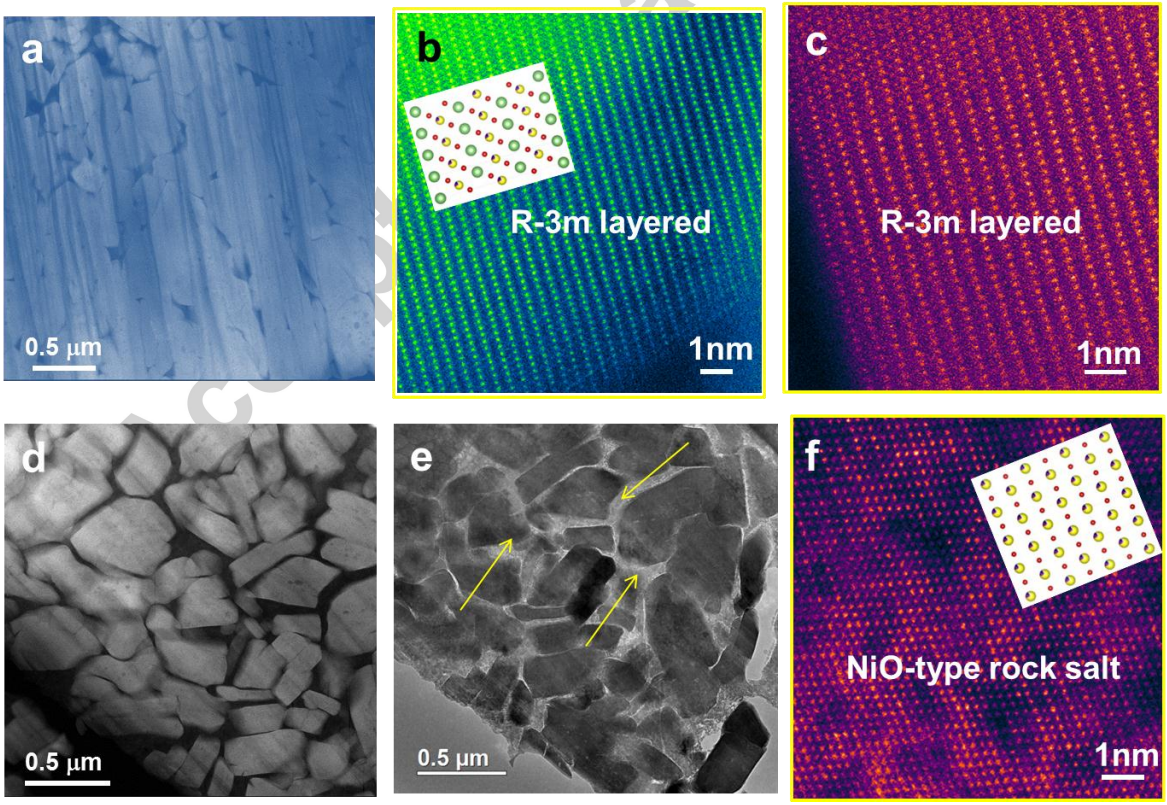

ACCEPTED MANUSCRIPT

Fig. 5. (a) STEM-HAADF imaging and (b, c) atomic level STEM-HAADF imaging of for pristine $LiNi_{0.76}Mn_{0.14}Co_{0.10}O_2$ material prepared at 750 ^{o}C; (d) STEM-HAADF imaging, (e) bright-field TEM imaging, and (f) STEM-HAADF imaging of for cycled $LiNi_{0.76}Mn_{0.14}Co_{0.10}O_2$ material (prepared at 750 ^{o}C) after 200 cycles at C/3 in the voltage range of 2.7~4.3 V. Insets in (b) and (f) are the atomic models showing the R-3m layered structures viewed down from [100] zone axis and Fd-3m viewed down from the [110] zone axis, respectively.

For further insight into the effect of calcination temperature, EIS was carried out to study the interfacial electrochemistry and reaction kinetics of the materials prepared at 750, 850, and 900 °C during cycling. The impedance spectra recorded at different cycles are shown in Fig. 6; these exhibit high-frequency semicircles, intermediate-frequency semicircles, and low-frequency tails. Generally, the high-frequency semicircle is related to the resistance arising from the passivation surface film (R_{sf}) or SEI layer [44,45]. The intermediate-frequency semicircle is associated with the charge-transfer resistance (R_{ct}) at the electrode/electrolyte interface coupled with a double-layer capacitance. The low-frequency tail is associated with Li^+ ion diffusion in the active electrode particles.

Accepted manuscript

ACCEPTED MANUSCRIPT

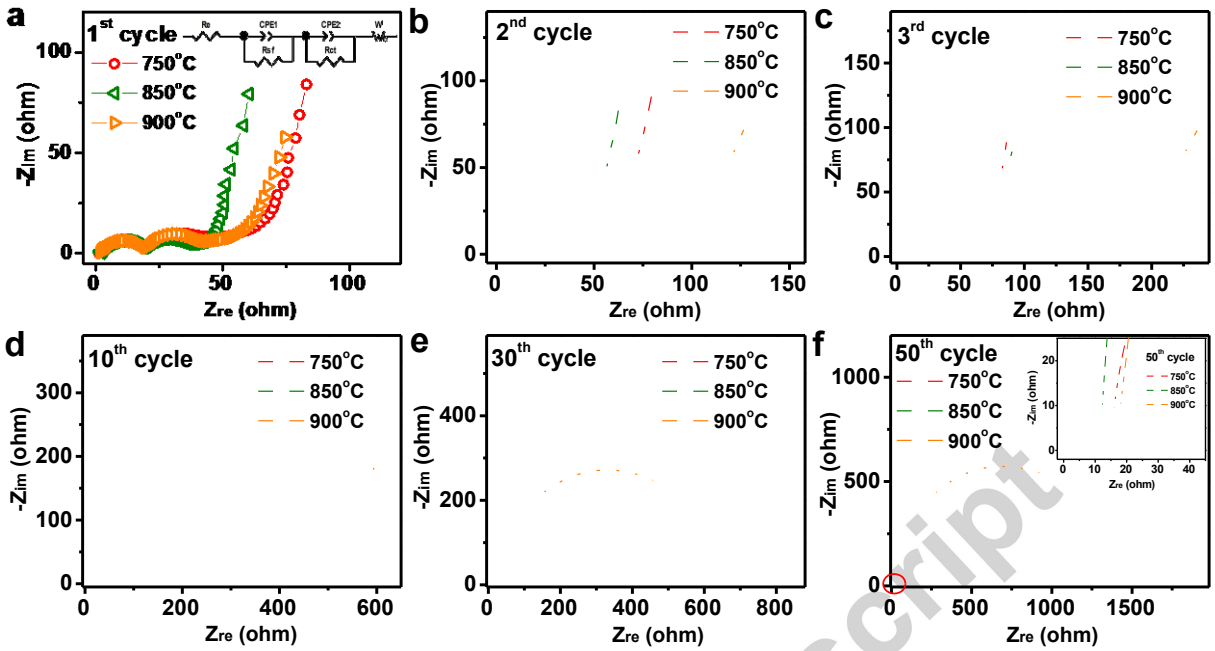

Fig. 6. Nyquist Plots of the $LiNi_{0.76}Mn_{0.14}Co_{0.10}O_2$ cathodes calcined at different temperatures in the charged state of 4.3 V during cycling. (a) 1st cycle; (b) 2nd cycle; (c) 3rd cycle; (b) 10th cycle; (e) 30th cycle; (f) 50th cycle. The inset in (f) is an enlargement of the high-frequency region of the EIS spectra at the 50th cycle. Inset in (a) is the equivalent circuit used for fitting the impedance spectra.

The impedance spectra were fitted using the equivalent circuit as inset in Fig. 6a, and the fitting results are tabulated in Table S1. During the first cycle, very little difference is observed for the cells charged to 4.3 V, indicating similar R_{sf} and R_{ct} (Fig. 6a). Upon cycling, the three materials show similar SEI layer resistance at different stages of cycling. In addition, the SEI layer resistance does not change much, and only accounts for a small portion of the total resistance of the cells. Therefore, the continuous increase of R_{ct} is considered the main reason for the capacity fade of the different materials. The materials prepared at higher temperatures of 850 and 900 °C present a rapid increase of R_{ct} during cycling (Fig. 6b-f). At the 50th cycle, the R_{ct} values of materials prepared at 850 and 900 °C are estimated to be ~872 and ~1501 Ω,

Accepted manuscript

ACCEPTED MANUSCRIPT

respectively, which are much higher than that for material prepared at 750 °C (~310 Ω). The significant increase in R_{ct} of materials prepared at 850 and 900 °C greatly increases the kinetic barrier for reversible lithium extraction/insertion, thereby leading to fast capacity degradation. This result coincides well with the serious micro-strain and -crack formation occurring in these two materials after cycling, causing loss of electrical contact between primary particles and thus increasing the R_{ct}.

The lithium-ion diffusion coefficient can be further calculated using the equation ($D = R^2T^2/2A^2n^4F^4c^2\sigma_\omega^2$), where σ_w is the Warburg impedance coefficient which can be obtained from the slope of $Z_{re} - \omega^{-1/2}$ relationship at low frequency (as shown in Fig. S4), D is lithium-ion diffusion coefficient, R is the gas constant, T is the absolute temperature, A is the electrode area, n is the number of electron transferred per molecule during the electrochemical reactions, F is Faraday constant, and c is molar concentration of Li^+. The lithium ion diffusion coefficients calculated at different stages of cycling are summarized in Table 2. Although the material prepared at 750 ^oC shows similar Li^+ ion diffusion coefficient compared with other materials at the early stage of cycling, it shows much slower increase of Li^+ ion diffusion coefficient after cycling. At 50th cycle, the Li^+ ion diffusion coefficient of material prepared at 750 ^oC (3.94×10^{-10}) is significantly higher than those prepared at 850 ^oC (5.26×10^{-11}) and 900 ^oC (8.21×10^{-12}). The results confirm the better structural integrity of material prepared at 750 ^oC because of the less cracks formation and the mitigated structural degradation during cycling process.

Table 2. Li^+ ion diffusion coefficients at different stages of cycling calculated on the basis of EIS method

Lithium ion diffusion coefficient ($cm^2\ s^{-1}$)

ACCEPTED MANUSCRIPT

	750 °C	850 °C	900 °C
1st cycle	8.08×10^{-9}	6.77×10^{-9}	6.66×10^{-9}
2nd cycle	3.87×10^{-9}	4.58×10^{-9}	1.99×10^{-9}
3rd cycle	3.76×10^{-9}	3.03×10^{-9}	6.27×10^{-10}
10th cycle	9.82×10^{-10}	2.99×10^{-10}	6.86×10^{-11}
30th cycle	9.76×10^{-10}	1.46×10^{-10}	4.89×10^{-11}
50th cycle	3.94×10^{-10}	5.26×10^{-11}	8.21×10^{-12}

The cycling performance of the $LiNi_{0.76}Mn_{0.14}Co_{0.10}O_2$ cathodes calcined at different temperatures was also evaluated under harsh testing conditions by cycling at an elevated temperature of 60 °C. The cycling result is shown in Fig. 7, and the corresponding voltage profile evolutions are compared in Fig. S5. These Ni-rich cathode materials had higher discharge capacities at 60 °C, suggesting an improvement in electrode kinetics during charge/discharge processes at elevated temperatures. Slightly lower initial discharge capacities are observed for the materials prepared at 725 or 900 °C (Fig. 7a), again reflecting either the poor crystallinity of the 725 °C sample or the long lithium-ion diffusion pathways in the 900 °C sample. Owing to the enhanced electrode kinetics, a high discharge capacity of ca. 230 mAh g^{-1} could be achieved for materials prepared at 750~850 °C, which corresponds to a high utilization of 84% of the total lithium content of the Ni-rich cathodes.

Accepted manuscript

ACCEPTED MANUSCRIPT

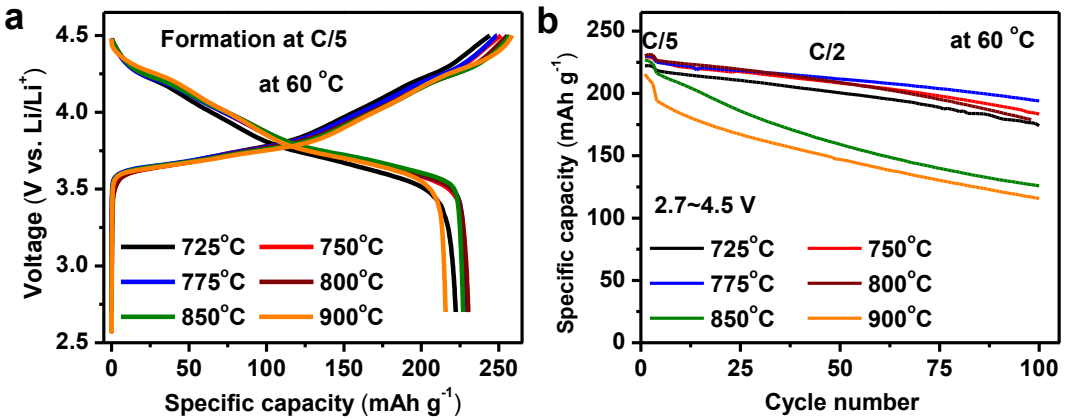

Fig. 7. (a) Charge/discharge profiles and (b) cycling performance of the $LiNi_{0.76}Mn_{0.14}Co_{0.10}O_2$ cathodes calcined at different temperatures and tested at high temperature (60 °C) at C/2 rate after 3 formation cycles at C/5.

As compared to those cycled at room temperature (Fig. 3), the materials show faster capacity degradation due to faster parasitic reactions and structural degradation during cycling at 60 °C (Fig. 7b). After 100 cycles, the capacity retention values of these materials are calculated to be 79.8%, 81.4%, 86.2%, 78.4%, 58.2%, and 59.6% for materials prepared at 725, 750, 775, 800, 850, and 900 °C, respectively. The material prepared at 775 °C exhibits the best capacity retention and the highest discharge capacity (194 mAh g^{-1}) after 100 cycles, benefiting from its superior structural properties such as good crystallinity, low Li/Ni cation mixing, and optimum primary particle size. The materials prepared at 850 and 900 °C again show fast capacity degradation during cycling. There is not much difference in BET surface area among all the materials (Table 1), so parasitic reactions between electrode material and electrolyte should be similar during cycling. The faster capacity degradation of materials calcined at high temperatures is then attributed to the rapid increase of electrode resistance arising from the large internal strain generated during repeated charge/discharge processes and the consequent contact loss between primary particles.

Accepted manuscript

ACCEPTED MANUSCRIPT

Rate performance of the $LiNi_{0.76}Mn_{0.14}Co_{0.10}O_2$ cathodes calcined at different temperatures was also tested, and the results are presented in Fig. 8. The sample prepared at 750 °C shows higher discharge capacities at various C rates (Fig. 8a). In particular, the sample delivers the highest discharge capacity of 168 mA h g^{-1} at a 10C rate, which is much higher than those of 152, 164, 163, 125 and 47 mA h g^{-1} for those prepared at 725, 775, 800, 850 and 900 °C, respectively. The poor rate capability of the material prepared at high calcination temperature, i.e., 850 or 900 °C, is attributed to the large kinetic barrier associated with the long lithium-ion diffusion pathway in the micron-size primary particles. The charge/discharge voltage profiles at different C rates show that materials calcined at temperatures ≥800 °C exhibit discharge voltage profiles with considerably lower working voltage at increasing C rates (Fig. 8c, d). This result suggests a significant increase in electrode resistance and a serious energy fade when discharging at higher current densities, which is unfavorable for practical applications in EVs and power tools. On the other hand, the material prepared at 750 °C shows very limited decrease in working voltage even at a 10C discharge rate (Fig. 8b), further demonstrating the structural advantages of this material.

Accepted manuscript

ACCEPTED MANUSCRIPT

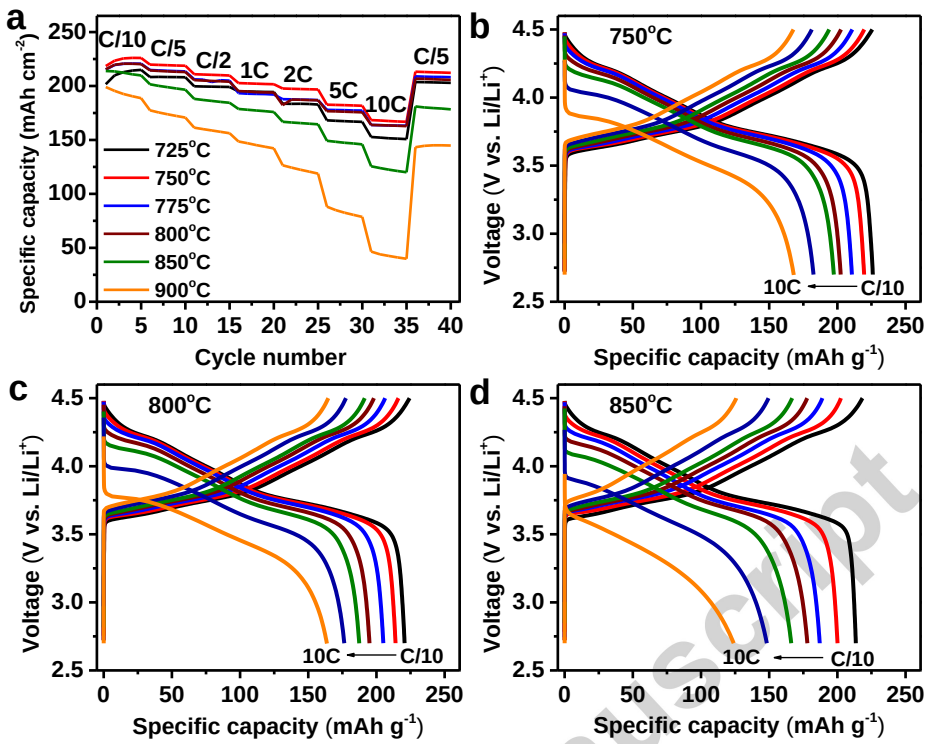

Fig. 8. (a) Rate performance of $LiNi_{0.76}Mn_{0.14}Co_{0.10}O_2$ cathodes calcined at different temperatures and the corresponding discharge profiles of materials prepared at (b) 750 °C, (c) 800 °C, and (d) 850 °C.

Because high areal capacity is required for practical applications, the electrochemical performance of the $LiNi_{0.76}Mn_{0.14}Co_{0.10}O_2$ sample prepared at 750 °C was also evaluated in thick electrode laminates with a loading of ca. 2.5 mAh cm^{-2} (~12 mg active material per cm^2), as shown in Fig. 9. The thick electrode still delivers a high discharge capacity of ca. 210 mAh g^{-1} during the formation cycles (Fig. 9a), which is similar to that obtained in a thin electrode with a low loading of 4–5 mg cm^{-2} as discussed above, indicating good electrode kinetics. During cycling at C/3 charge rate and 1C discharge rate, the thick $LiNi_{0.76}Mn_{0.14}Co_{0.10}O_2$ electrode behaves similarly to its thin-electrode counterpart, demonstrating good cycling stability with a high capacity retention of 92% after 100 cycles (Fig. 9b). Besides, a full cell using commercial

Accepted manuscript

ACCEPTED MANUSCRIPT

graphite anode (Mag10 of 1.5 mAh cm^{-2} provided from Argonne National Lab) further demonstrates that the graphite||$LiNi_{0.76}Mn_{0.14}Co_{0.10}O_2$ can achieve a high discharge capacity of 201 mAh g^{-1} and a capacity retention up to 78.3% after 700 cycles at 1C rate (Fig. S6). The superior electrochemical performance of the $LiNi_{0.76}Mn_{0.14}Co_{0.10}O_2$ (prepared at the optimum temperature) validates it as a promising cathode material for next-generation high energy density LIBs.

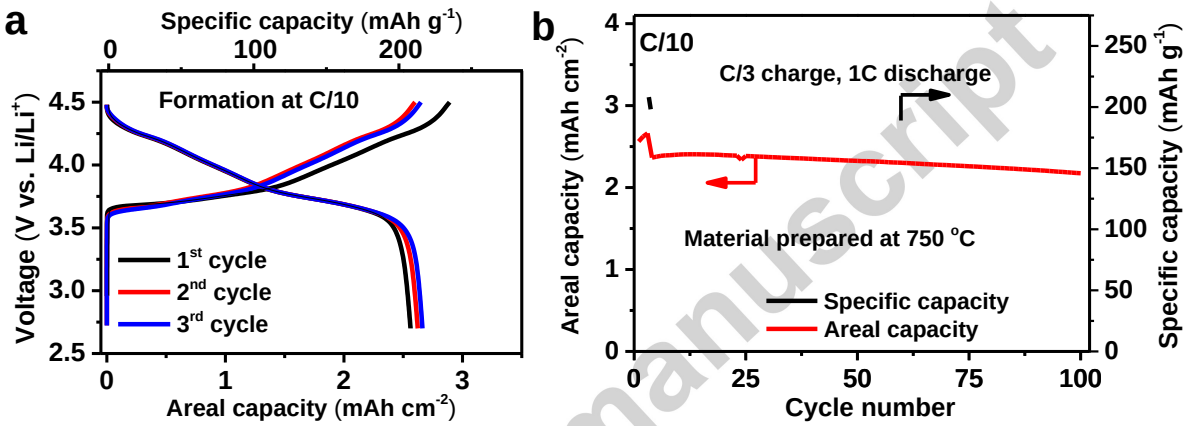

Fig. 9. (a) Voltage profiles versus areal capacity and specific capacity, (b) areal and specific capacity as a function of cycle number of $LiNi_{0.76}Mn_{0.14}Co_{0.10}O_2$ prepared at 750 °C in thick electrodes of about 12 mg active material per cm^2.

Accepted manuscript

4. Conclusion

The effect of calcination temperature on the structure, morphology, and electrochemical performance of Ni-rich $LiNi_{0.76}Mn_{0.14}Co_{0.10}O_2$ cathode materials at a high charge cutoff voltage of 4.5 V has been systematically investigated. The results demonstrate that the electrochemical performance of Ni-rich cathodes is sensitive to the calcination temperature and the primary particle size. The best performing $LiNi_{0.76}Mn_{0.14}Co_{0.10}O_2$ cathode material was achieved when it was calcined at 750~775 °C (100~300 nm primary particle size); it is capable of delivering a capacity above 160 mAh g^{-1} at 10C rate and retaining ca. 79% of its initial capacity after 200

ACCEPTED MANUSCRIPT

cycles at C/3. Higher calcination temperature (≥800 °C) leads to inferior long-term cycling stability and rate capability because of severe micro-strain and -crack formation upon lithium-ion de/intercalation that is closely related to the large primary particles (even >1 μm) in the material, in which the primary particle size increases. The findings highlight the importance of optimizing the synthetic conditions for preparing the Ni-rich cathode materials. The optimum calcination temperatures & primary particle size would depend on the compositions of the Ni-rich cathodes, which need to be carefully considered for the synthesis of other Ni-rich cathode materials in order to maximize their electrochemical performance.

Accepted manuscript

Acknowledgment

This work is supported by the Assistant Secretary for Energy Efficiency and Renewable Energy, Office of Vehicle Technologies of the U. S. Department of Energy (DOE) under Contract No. DE-AC02-05CH11231, Subcontract No. 18769, under the Advanced Battery Materials Research (BMR) program. The SEM morphology observations were conducted in the William R. Wiley Environmental Molecular Sciences Laboratory (EMSL), a national scientific user facility sponsored by DOE's Office of Biological and Environmental Research and located at PNNL. PNNL is operated by Battelle for the DOE under Contract DE-AC05-76RL01830.

Appendix A. Supporting information

Supplementary data associated with this article can be found in the online version at http://dx.doi.org/10.1016/j.nanoen.201x.xx.xxx.

ACCEPTED MANUSCRIPT

References

[1] J.M. Tarascon, M. Armand, Nature 414 (2001) 359–367.

[2] J.B. Goodenough, H.D. Abruña, M.V. Buchanan, S. Visco, M.S. Whittingham, B. Dunn, Y. Gogotsi, A. Gewirth, D. Nocera, (2007) http://web.anl.gov/energy-storage-science/publications/EES_rpt.pdf.

[3] L.-F. Cui, Y. Yang, C.-M. Hsu, Y. Cui, Nano Lett. 9 (2009) 3370–3374.

[4] M.S. Whittingham, Proc. IEE 100 (2012) 1518–1534.

[5] M.M. Thackeray, S.-H. Kang, C.S. Johnson, J.T. Vaughey, R. Benedek, S.A. Hackney, J. Mater. Chem. 17 (2007) 3112–3125.

[6] J. Zheng, J. Xiao, X. Yu, L. Kovarik, M. Gu, F. Omenya, X. Chen, X.-Q. Yang, J. Liu, G.L. Graff, M.S. Whittingham, J.-G. Zhang, Phys. Chem. Chem. Phys. 14 (2012) 13515–13521.

[7] Y.-K. Sun, Z. Chen, H.-J. Noh, D.-J. Lee, H.-G. Jung, Y. Ren, S. Wang, C.S. Yoon, S.-T. Myung, K. Amine, Nat Mater 11 (2012) 942–947.

[8] Y.-K. Sun, S.-T. Myung, B.-C. Park, J. Prakash, I. Belharouak, K. Amine, Nat Mater 8 (2009) 320–324.

[9] W. Liu, P. Oh, X. Liu, M.-J. Lee, W. Cho, S. Chae, Y. Kim, J. Cho, Angew. Chem. Int. Ed. 54 (2015) 4440–4457.

[10] A. Manthiram, J.C. Knight, S.-T. Myung, S.-M. Oh, Y.-K. Sun, Adv. Energy Mater. 6 (2016) 1501010.

[11] Y. Wei, J. Zheng, S. Cui, X. Song, Y. Su, W. Deng, Z. Wu, X. Wang, W. Wang, M. Rao, Y. Lin, C. Wang, K. Amine, F. Pan, J. Am. Chem. Soc. 137 (2015) 8364–8367.

[12] B. Huang, X. Li, Z. Wang, H. Guo, X. Xiong, Ceram. Int. 40 (2014) 13223–13230.

[13] P. Yue, Z. Wang, H. Guo, X. Xiong, X. Li, Electrochim. Acta 92 (2013) 1–8.

Accepted manuscript

ACCEPTED MANUSCRIPT

[14] H. Kim, M.G. Kim, H.Y. Jeong, H. Nam, J. Cho, Nano Lett. 15 (2015) 2111–2119.

[15] Y. Cho, P. Oh, J. Cho, Nano Lett. 13 (2013) 1145–1152.

[16] S.H. Ju, I.-S. Kang, Y.-S. Lee, W.-K. Shin, S. Kim, K. Shin, D.-W. Kim, ACS Appl. Mater. Interfaces 6 (2014) 2546–2552.

[17] X. Xiong, Z. Wang, G. Yan, H. Guo, X. Li, J. Power Sources 245 (2014) 183–193.

[18] J. Zheng, W.H. Kan, A. Manthiram, ACS Appl. Mater. Interfaces 7 (2015) 6926–6934.

[19] S.-J. Yoon, K.-J. Park, B.-B. Lim, C.S. Yoon, Y.-K. Sun, J. Electrochem. Soc. 162 (2015) A3059–A3063.

[20] J. Yang, M. Hou, S. Haller, Y. Wang, C. Wang, Y. Xia, Electrochim. Acta 189 (2016) 101–110.

[21] J. Yang, Y. Xia, ACS Appl. Mater. Interfaces 8 (2016) 1297–1308.

[22] M.-H. Choi, C.S. Yoon, S.-T. Myung, B.-B. Lim, S. Komaba, Y.-K. Sun, J. Electrochem. Soc. 162 (2015) A2313–A2318.

[23] I. Hwang, C.W. Lee, J.C. Kim, S. Yoon, Mater. Res. Bull. 47 (2012) 73–78.

[24] C. Fu, G. Li, D. Luo, Q. Li, J. Fan, L. Li, ACS Appl. Mater. Interfaces 6 (2014) 15822–15831.

[25] F. Wu, J. Tian, Y. Su, J. Wang, C. Zhang, L. Bao, T. He, J. Li, S. Chen, ACS Appl. Mater. Interfaces 7 (2015) 7702–7708.

[26] X.-q. Li, X.-h. Xiong, Z.-x. Wang, Q.-y. Chen, Trans. Nonferrous Met. Soc. China 24 (2014) 4023–4029.

[27] J.-Z. Kong, F. Zhou, C.-B. Wang, X.-Y. Yang, H.-F. Zhai, H. Li, J.-X. Li, Z. Tang, S.-Q. Zhang, j. alloys. compd. 554 (2013) 221-226.

Accepted manuscript

ACCEPTED MANUSCRIPT

[28] J.-H. Shim, C.-Y. Kim, S.-W. Cho, A. Missiul, J.-K. Kim, Y.J. Ahn, S. Lee, Electrochim. Acta 138 (2014) 15–21.

[29] Y. Bi, W. Yang, R. Du, J. Zhou, M. Liu, Y. Liu, D. Wang, J. Power Sources 283 (2015) 211–218.

[30] J. Zheng, J. Xiao, J.-G. Zhang, Nano Today 11 (2016) 678–694.

[31] C.S. Johnson, N. Li, C. Lefief, J.T. Vaughey, M.M. Thackeray, Chem. Mater. 20 (2008) 6095-6106.

[32] A.L. Patterson, Phys. Rev. 56 (1939) 978–982.

[33] L. Tan, H. Liu, Solid State Ionics 181 (2010) 1530–1533.

[34] N. Yabuuchi, T. Ohzuku, J. Power Sources 119–121 (2003) 171–174.

[35] J.K. Ngala, N.A. Chernova, M. Ma, M. Mamak, P.Y. Zavalij, M.S. Whittingham, J. Mater. Chem. 14 (2004) 214–220.

[36] J. Zheng, P. Xu, M. Gu, J. Xiao, N.D. Browning, P. Yan, C. Wang, J.-G. Zhang, Chem. Mater. 27 (2015) 1381–1390.

[37] J. Zheng, S. Myeong, W. Cho, P. Yan, J. Xiao, C. Wang, J. Cho, J.-G. Zhang, Adv. Energy Mater. 7 (2017) 1601284.

[38] S. Zheng, R. Huang, Y. Makimura, Y. Ukyo, C.A.J. Fisher, T. Hirayama, Y. Ikuhara, J. Electrochem. Soc. 158 (2011) A357–A362.

[39] D.J. Miller, C. Proff, J.G. Wen, D.P. Abraham, J. Bareño, Adv. Energy Mater. 3 (2013) 1098–1103.

[40] E.-J. Lee, Z. Chen, H.-J. Noh, S.C. Nam, S. Kang, D.H. Kim, K. Amine, Y.-K. Sun, Nano Lett. 14 (2014) 4873–4880.

Accepted manuscript

ACCEPTED MANUSCRIPT

[41] H. Liu, M. Wolf, K. Karki, Y.-S. Yu, E.A. Stach, J. Cabana, K.W. Chapman, P.J. Chupas, Nano Lett. 17 (2017) 3452–3457.

[42] Y. Hu, X. Zhao, Z. Suo, J. Mater. Res. 25 (2010) 1007–1010.

[43] Y. Hu, X. Zhao, Z. Suo, J. Mater. Res. 25 (2011) 1007-1010.

[44] F. Nobili, F. Croce, B. Scrosati, R. Marassi, Chem. Mater. 13 (2001) 1642–1646.

[45] J. Zheng, X. Wu, Y. Yang, Electrochim. Acta 105 (2013) 200–208.

Accepted manuscript

ACCEPTED MANUSCRIPT

Dr. Jianming Zheng is currently a manager of Research Institute (RI) of Ningde Amperex Technology Limited (ATL). Before joining ATL recently, he was a staff scientist of the Pacific Northwest National Laboratory. Dr. Zheng has extensive experience in the development of high-energy cathode materials for Li-ion batteries, the development of high performance electrolytes/additives for Li-ion batteries, and the protection of Li metal anode for rechargeable Li metal batteries. He also has experience in the development of Li-S batteries, and sodium ion batteries. Dr. Zheng has more than 90 papers published in peer-reviewed professional journals, and holds 2 US patents.

Dr. Pengfei Yan was a research associate in the Environmental Molecular Sciences Laboratory, Pacific Northwest National Laboratory (2013.11~2017.6). He received his Ph.D. in 2010 from Institute of Metal Research, Chinese Academy of Sciences. Now Dr. Yan is a professor of Beijing University of Technology in China, his research interests are mainly focused on energy materials by using advanced electron microscopy.

Luis completed his Ph.D. in Materials Science and Engineering at Cornell University, where Luis worked under the mentorship of Dr. Emmanuel Giannelis on porous/composite materials for use as PEM fuel cell electrodes and eventually high surface area porous carbon materials for energy storage devices such as Li-S battery and supercapacitors. After completing his Ph.D., Luis successfully obtained a Linus Pauling Distinguished Fellowship to develop hierarchical porous structured materials at Pacific Northwest National Laboratory for applications targeting energy storage. Luis is currently a Battery Scientist in the Solid-State Battery and Integrated Systems team at the University of Dayton Research Institute.

Accepted manuscript

ACCEPTED MANUSCRIPT

Chongmin Wang is a staff scientist at Environmental Molecular Sciences Laboratory, Pacific Northwest National Laboratory. His research is focused on S/TEM, especially in-situ S/TEM and energy materials. Before Joining PNNL, he worked at Max-Planck Institute for Metal Research in Stuttgart of Germany, NIMS of Japan, and Lehigh University of USA. He is the recipients of MRS Innovation in Materials Characterization Award, *JMR* Paper of the Year Award, Microscopy Today Innovation Award, Rowland Snow Award (American Ceramic Society), R&D100 Award, Outstanding Invention Award (Japan), and PNNL Directors Award for Exceptional Scientific Achievement. He is a Fellow of MRS.

Dr. Ji-Guang (Jason) Zhang is a Laboratory Fellow of the Pacific Northwest National Laboratory. He is the group leader for PNNL's efforts in energy storage for transportation applications and has 26-year experience in the development of energy storage devices, including Li-ion batteries, Li-metal batteries, Li-air batteries, Li-S batteries, and thin-film solid-state batteries. He was the co-recipient of two R&D 100 awards, holds 23 patents (with another 31 patents pending) and publishes more than 250 papers in refereed journals. He was named Highly Cited Researchers-2017 in both Materials Science and Engineering category.

Accepted manuscript

Highlights

- Temperatures of 750~775 °C are optimum for calcining Ni-rich $LiNi_{0.76}Mn_{0.14}Co_{0.10}O_2$ (NMC76) materials.

ACCEPTED MANUSCRIPT

- The primary particle size of Ni-rich cathode materials was controlled by the calcination temperature.
- The size of primary particles showed significant effects on the structural integrity of secondary particles of Ni-rich cathode materials.
- Ni-rich materials constructed with primary particles of about 100–300 nm exhibited the best electrochemical performance.

Accepted manuscript